J. Zhang
Graduate Research Assistant, Department of Mechanical Engineering and Applied Mechanics.

Z. Lin
Research Fellow, Department of Civil and Environmental Engineering.

A. Wong
Graduate Research Assistant, Department of Civil and Environmental Engineering.

N. Kikuchi
Professor, Department of Mechanical Engineering and Applied Mechanics.

V. C. Li
Professor, Department of Civil and Environmental Engineering.

A. F. Yee
Professor, Department of Material Science and Engineering.

The University of Michigan, Ann Arbor, MI 48109

G. S. Nusholtz
Chrysler Corporation, Auburn Hills, MI 48326

Constitutive Modeling and Material Characterization of Polymeric Foams

In this study, mechanical properties of three types of polymeric foams (polypropylene (PP), polystyrene (PS), and polyurethane (PU) foams) are investigated. Focus has been placed on the strain rate and temperature effects on these foams under large deformations. Selected experimental results from uniaxial compression, hydrostatic compression, and simple shear tests are presented. A phenomenological hydrodynamic elastoplastic constitutive law is developed to model these polymeric foams. Numerical implementation and validation of the constitutive model are also described.

1 Introduction

Polymeric foams are excellent energy absorbers and have found a wide range of applications, especially in the automotive industry. New provisions in the Federal Motor Vehicle Safety Standards 201 (FMVSS) require the use of Head Injury Criterion (HIC) for a free motion head form which impacts the interior of the vehicle. To satisfy such a criterion, polymeric foams are currently being considered as viable vehicle interior padding materials. In such an application, polymeric foams are usually subjected to large deformations under high deformation rates. A typical computer-aided interior padding design process involves finite element simulation of the impact between crash test dummy and vehicle interior trim components (Bilkhu et al., 1993; Chang et al., 1994; Barbat and Prasad, 1995). Hence material characterization and constitutive modeling of these foam materials are essential.

Polymeric foams consist of large quantity of either open or closed cells. Figure 1 shows the microstructures of three types of foam materials under current investigation. The PP foam is a closed-cell semi-rigid foam with density 3.06 pcf (pound per cubic foot). Note that it has a bi-level structure of cells. The PU is an open-cell flexible foam with density 6.0 pcf and the PS (1.0 pcf) is a rigid foam with equal-sized, closed cells.

A typical stress-strain curve of a polymeric foam exhibits three regimes (Gibson and Ashby, 1988): a linear elastic regime (due to cellular wall bending) at low stresses followed by a long collapse plateau and a densification regime in which the stress rises steeply. The mechanisms associated with the collapse plateau are different, depending on the properties of the cell walls. For flexible foams, the collapse plateau is due to elastic buckling of cell walls. For rigid and brittle foams, plastic yielding and brittle crushing of the cell walls are the main failure mechanisms respectively. Under tension, on the other hand, the post-elasticity behavior of a polymeric foam is controlled by cell wall alignment towards the loading axis and the stress-strain curve is ultimately truncated by either ductile or brittle fracture. Extensive analytical and experimental work has been carried out to characterize the elastic and failure behaviors of polymeric foams (Gibson and Ashby, 1988; Gibson et al., 1989; Triantafillou et al., 1989; Triantafillou and Gibson, 1990). Puso and Govindjee (1995) used a modified version of the multi-surface failure criterion by Gibson and co-workers and developed an orthotropic rate-independent plasticity and viscoplasticity constitutive law for rigid foams.

The strain-rate, hydrostatic pressure, and temperature effects are important aspects to be considered in the applications of polymeric foams. The microstructural features of polymeric foams (e.g., cell configuration, cell size, strut thickness, etc.) lead to more complexity in material property characterization as compared to solid polymers. Gibson and Ashby (1988) reviewed the work of a number of other authors on elastic, visco-

Contributed by the Materials Division for publication in the JOURNAL OF ENGINEERING MATERIALS AND TECHNOLOGY. Manuscript received by the Materials Division December 19, 1996; revised manuscript received April 23, 1997. Associate Technical Editor: L. Catherine Brinson.

Fig. 1(a)

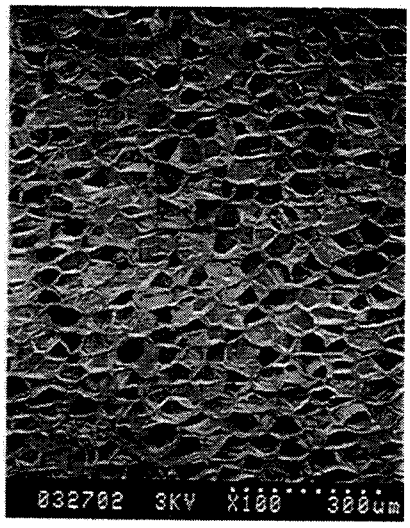

Fig. 1(b)

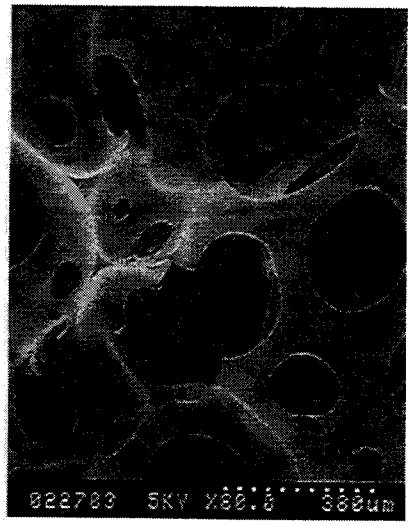

Fig. 1(c)

Fig. 1 The microstructure of (a) a closed-cell semi-rigid PP foam (3.06 pcf), (b) a closed-cell rigid PS foam (1.0 pcf), and (c) an open-cell flexible PU foam (6.0 pcf)

elastic, plastic yielding and creep responses of both open and closed cell foams.

The purpose of this research is to investigate the strain rate, hydrostatic pressure, and temperature dependent behaviors of polymeric foams used in the automotive industry and to develop a phenomenological constitutive model for computer simulation of crash impacts, in which compression and shear are the dominant deformation modes while tension is less relevant. The model will be further implemented into a dynamic finite element analysis code such as LS-DYNA3D (Hallquist, 1994). This paper presents an integrated experimental, theoretical and numerical approach in achieving this objective.

The remainder of this paper is organized as follows. In Section 2, the experimental program and test results are presented. The experimental results include: (1) uniaxial compression tests on the PP (3.06 pcf), PS (1.0 pcf), and PU (6.0 pcf) foams; (2) hydrostatic compression tests on the PP (3.06 pcf) and PU (6.0 pcf) foams; and (3) simple shear tests on the PS foam (1.0 pcf). Temperature effect on polypropylene (3.06 pcf) foam has also been investigated. An empirical constitutive law is proposed to account for both strain rate and temperature dependence for foams under uniaxial compression. In Section 3, a phenomenological hydrodynamic elastoplastic formulation is presented to model the constitutive behavior of rigid foams. Numerical implementation procedures of the constitutive equation and simulation results are given in Section 4. Conclusions from this study are summarized in Section 5.

2 Experimental Investigations

2.1 Experimental Program. Experiments, including uniaxial compression, hydrostatic compression and simple shear, were conducted on: (1) an electro-hydraulic Instron 1331 machine equipped with a temperature chamber, and (2) a pneumatically driven ICI instrumented impact machine (used for uniaxial compression only). The Instron 1331 testing machine can maintain constant cross-head speeds ranging from quasi-static (0.08 mm/sec, ASTM Standard D1621) to 250 mm/sec with a closed-loop servo-controlled system. The pneumatically driven ICI machine can achieve initial impact speed of up to 10 m/s. Although the impactor speed of the ICI impact machine is varying during the impact process, the recorded impactor velocity history showed a broad plateau which was used to compute the average strain rate.

Foam specimens are $50 \times 50 \times 50$ mm^3 in dimension for compression and tension tests and $50 \times 50 \times 100$ mm^3 for simple shear tests. Four different cross-head rates of 8.0×10^{-5} m/s, 4.0×10^{-3} m/s, 0.229 m/s, and 4.45 m/s (corresponding strain rates 1.6×10^{-3}, 0.08, 4.6, and 88/sec) were used in uniaxial compression tests.

For simple shear tests, foam specimens were glued in-between two L-shaped loading fixtures made of steel. The uniaxial tension fixture consists of two circular loading plates to which the top and the bottom of the test specimen are glued. During a hydrostatic compression test, foam specimens were wrapped by latex rubber and immersed into a specially-designed hydrostatic compression chamber filled with water. Air is allowed to escape from the specimens through an air vent on the lid of the chamber. This design is similar to the one by Triantafillou et al. (1989). All specimens were subjected to 80 percent volumetric strain in uniaxial and hydrostatic compression tests and loaded until fracture in tension and simple shear tests.

The tests conducted under various temperatures are for uniaxial compression only. The temperature range of −20°C to 80°C was selected.

2.2 Experimental Results. Under uniaxial compression, all foam specimens showed macroscopically uniform deformation without noticeable bulging and distortion. The Poisson's effect at large deformation is negligible, which is consistent

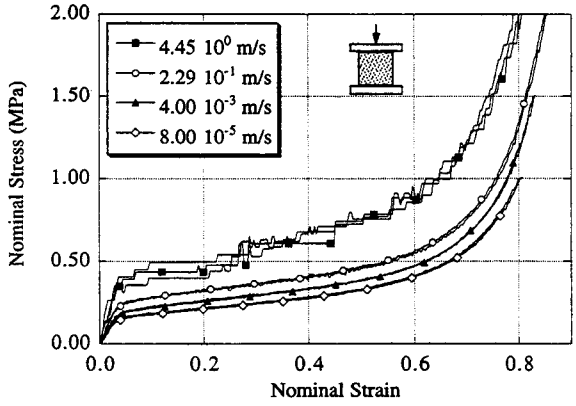

Fig. 2 Uniaxial compression stress-strain curves of polypropylene foam (3.06 pcf) under various strain rates at room temperature

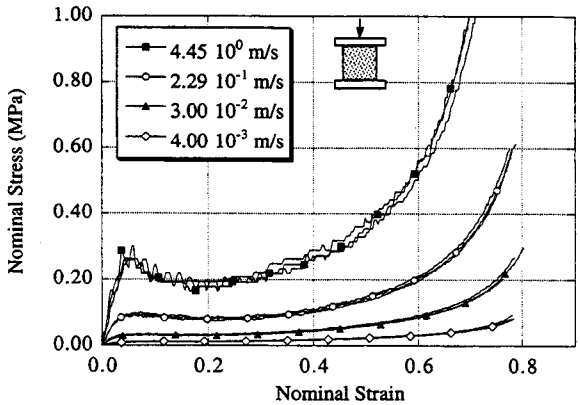

Fig. 4 Uniaxial compression stress-strain curves of polyurethane foam (6.0 pcf) under various strain rates at room temperature

with observations by other researchers (Shaw and Sata, 1966; Patel and Finnie, 1969; Gibson and Ashby, 1988). Experimental work also reveals that, at room temperature, the polypropylene foam (3.06 pcf) is a semi-rigid foam with only 20 percent permanent strain after unloaded from 80 percent applied strain. The polystyrene (1.0 pcf) foam is a rigid (crushable) foam with no resilience while polyurethane (6.0 pcf) is a flexible foam with full but retardative resilience.

Figures 2, 3, and 4 show the stress-strain responses of PP (3.06 pcf), PS (1.0 pcf) PU (6.0 pcf) and foams under uniaxial compression with different strain rates respectively. At least two tests were conducted at each rate to ascertain the data repeatability. It is clear that these curves consist of three regimes: (1) an approximate linear elastic regime due to cell wall elastic bending, (2) a plateau regime corresponding to cell wall buckling (for the flexible PU foam) or plastic yielding (for the rigid PP and PS foams), and (3) a steep hardening regime due to densification of the material. All three types of foams show distinctive strain-rate sensitivity. They are stiffer and stronger when subjected to higher strain rates. PU foam (6.0 pcf) appears to be the most sensitive to strain rate among three foams while the strain-rate sensitivity of the PS foam (1.0 pcf) becomes saturated beyond the strain rate of 4.6/s.

The stress-strain responses of PP and PU foams under hydrostatic compression have similar characteristics as that under uniaxial compression. They are also strain-rate dependent (see Figs. 5 and 6). Figure 7 shows the material response of the PS foam (1.0 pcf) under simple shear at different rates. The cut-off points are where specimens failed. Figures 8(a) and (b) show the temperature effects for the PP foam (3.06 pcf) under uniaxial compressive strain rates of 0.0016 and 4.6/s. As temperature increases from −20°C to 80°C, the stiffness and strength of the material decrease significantly. The energy absorption capacity is reduced as temperature rises.

2.3 Phenomenological Rate and Temperature Effect Modeling. The above experimental results have shown that the constitutive behaviors of polymeric foam materials are sensitive to the rate of deformation and temperature. Motivated by the work of Nagy et al. (1964) and the WLF equation, we propose the following phenomenological constitutive equation to account for both strain rate and temperature effects

$$\sigma(\epsilon) = \sigma_0(\epsilon)L(T)\left(\frac{\dot{\epsilon}}{\dot{\epsilon}_0}\right)^{a+b\epsilon} \tag{1}$$

where $\sigma_0(\epsilon)$ represents the engineering stress-engineering strain relation at an arbitrary quasi-static engineering strain rate $\dot{\epsilon}_0$. a and b are material constants. The temperature dependent function $L(T)$ is defined by the WLF shifting factor

$$L(T) = \exp\left[-\frac{C_1(T - T_r)}{C_2 + T - T_r}\right] \tag{2}$$

where C_1 and C_2 are material constants to be determined from temperature effect experiments. T_r is the room temperature (~25°C). When T equals to T_r, $L(T)$ becomes unity. Equation (1) is then reduced to

$$\sigma(\epsilon) = \sigma_0(\epsilon)\left(\frac{\dot{\epsilon}}{\dot{\epsilon}_0}\right)^{a+b\epsilon} \tag{3}$$

which represents the rate dependent stress-strain response at

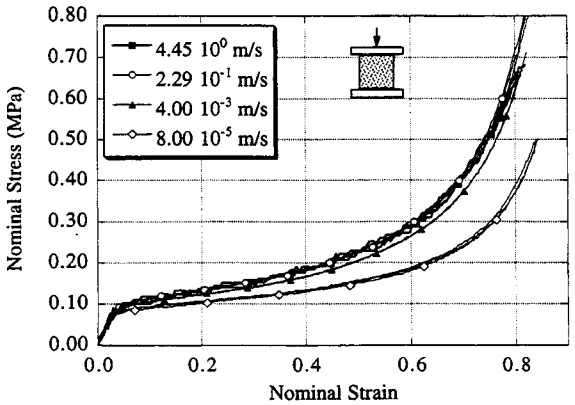

Fig. 3 Uniaxial compression stress-strain curves of polystyrene foam (1.0 pcf) under various strain rates at room temperature

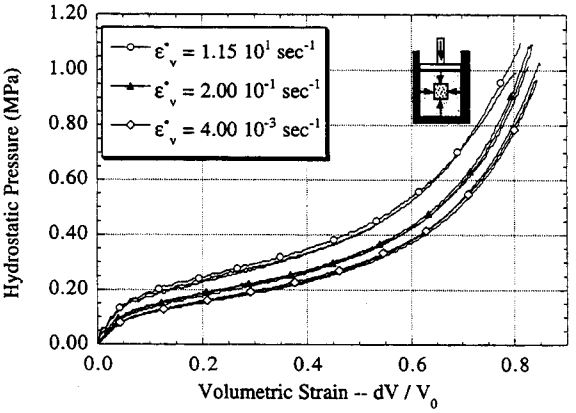

Fig. 5 Hydrostatic compression stress-strain curves of polypropylene foam (3.06 pcf) under various strain rates at room temperature

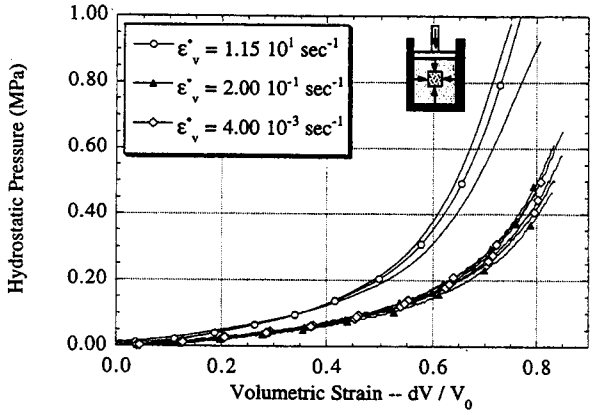

Fig. 6 Hydrostatic compression stress-strain curves polyurethane foam (6.0 pcf) under various strain rates at room temperature

room temperature. In order to obtain the material constants in Eq. (3), the nominal uniaxial stress σ is plotted against the nominal strain rate $\dot{\epsilon}$ on a log-log scale at different strain levels. Figure 9 shows the result for the PP foam (3.06 pcf). It is found that the data roughly form a family of straight lines each with a slope $n(\epsilon)$ which can be further fitted to a linear function $a + b\epsilon$. Table 1 summarizes the expressions of $n(\epsilon)$ for three types of foams under the present study.

To examine the validity of Eq. (1), the PP foam was used as an example. The material parameters C_1 and C_2 were determined from the quasi-static (0.0016/s) curves at −20°C and 80°C (Fig. 8(*a*)). The calculated values are: C_1 = 6.52°C and C_2 = 468.7°C. Figure 10 shows the comparison between model predictions and experimental data (Fig. 8(*b*)). Although Eq. (1) is empirical, it is found to be adequate to capture the strain rate and temperature dependence for the polymeric foams studied. It should be noted that while Eq. (1) implies that the elastic moduli of these foams are also rate-dependent as shown by our experimental results, it may or may not applicable to all other foams.

3 Constitutive Modeling

Mechanism-based constitutive models for polymeric foams have been well documented by Gibson and Ashby (1988). The failure envelope under multiaxial loading conditions has been derived by Gibson et al. (1989) and Triantafillou et al. (1989). Puso and Govindjee (1995) presented an orthotropic rate-independent plasticity and viscoplasticity formulation by extending the work by Gibson et al (1989) for rigid polymeric foams.

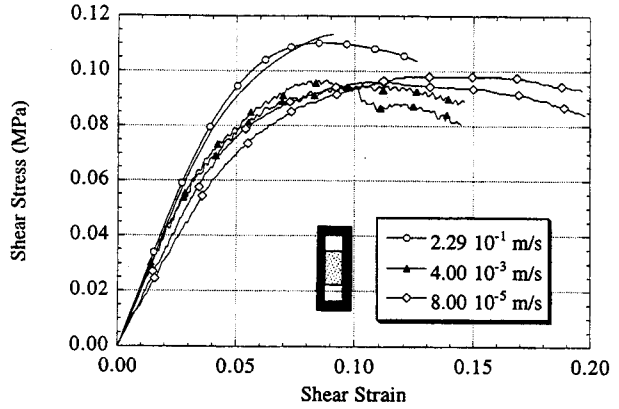

Fig. 7 Rate-dependent stress-strain responses of polystyrene foam (1.0 pcf) under simple shear

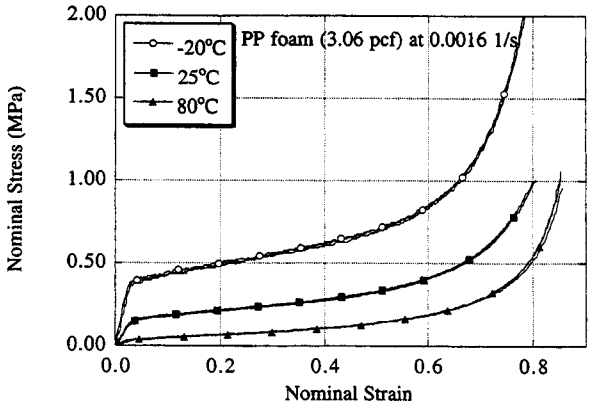

Fig. 8(*a*)

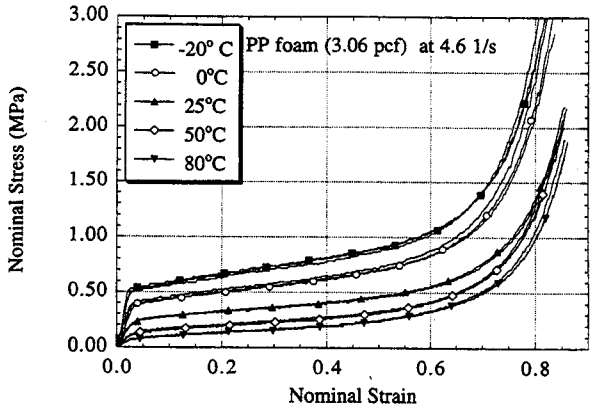

Fig. 8(*b*)

Fig. 8 Temperature effects on uniaxial compression responses of polypropylene foam (3.06 pcf): (*a*) under quasi-static strain rate 0.0016/s, (*b*) under 4.6/s strain rate

They further implemented the model in the computer code DYNA3D.

Other researchers have taken phenomenological approaches to develop equations which describe the inelastic response of foams under uniaxial compression (Rush, 1969; Ramon et al., 1990; Sherwood and Frost, 1992). Their approaches are accurate for predicting the response of foams in a specific uniaxial

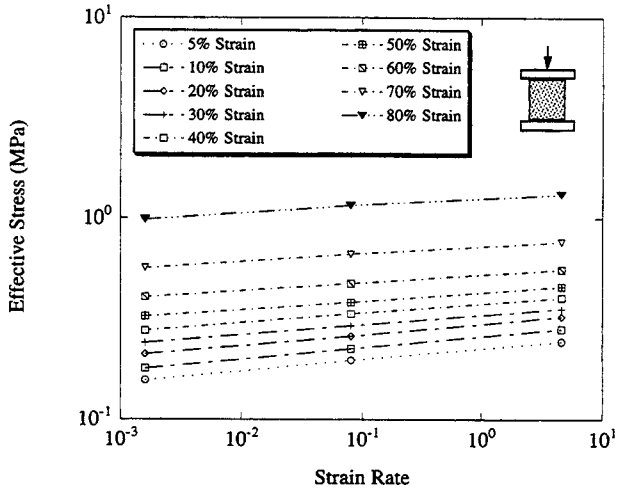

Fig. 9 Fitting the strain sensitivity parameter $n(\epsilon)$ for PP foam (3.06 pcf) at room temperature

Table 1 Strain rate sensitivity function $n(\epsilon)$ for various foams

Type of foam	$n(\epsilon)$
Polypropylene foam (3.06 pcf)	$0.037 + 0.0136\epsilon$
Polyurethane foam (6.0 pcf)	$0.307 + 0.1059\epsilon$
Polystyrene foam (1.0 pcf)	$0.016 + 0.0833\epsilon$

impact event but generally not applicable to multi-axial loading conditions.

Constitutive equations based on continuum constitutive theories have also been investigated. Roscoe's critical state theory (Schofield and Worth, 1968) has found successful application in soil mechanics. Krieg (1972) developed a plasticity theory for soils and crushable foams. This plasticity theory has a yield surface which is a parabola of revolution about the hydrostatic axis with a planar cap on the normally open end. Neilsen et al (1995) developed a plasticity theory for a semi-rigid polyurethane foams which has six intersecting planar yield surfaces forming a cubic shape in the principal stress space.

In the present study, a phenomenological single-surface yield criterion is constructed based on the experimental data presented in previous section. Comparisons with other yield criteria in the literature are made. Formulations for the strain and strain rate hardening are also presented.

3.1 Elastic Response. The initial stage of deformation of rigid foam is roughly linear elastic. Using the objective stress rate in a corotational reference system, the stress rate $\hat{\sigma}$ is decomposed into deviatoric and volumetric components

$$\hat{\sigma} = 2G(\hat{\epsilon}_d - \hat{\epsilon}_{dp}) - K(\dot{\epsilon}_v - \dot{\epsilon}_{vp})\hat{\mathbf{I}} \qquad (4)$$

where $\hat{\sigma}$ is an objective stress rate, $\hat{\epsilon}_d$, $\hat{\epsilon}_{dp}$, $\hat{\epsilon}_v$, and $\hat{\epsilon}_{vp}$ are deviatoric strain, plastic deviatoric strain, volumetric strain and plastic volumetric strain rate tensors, respectively.

3.2 Yield Criterion. The theoretical formulation of a multi-axial yield criterion for a polymeric foam is very complicated. The difficulty lies in the fact that "failure" (breakdown of linear elasticity) is associated with different mechanisms (i.e., plastic yielding, elastic buckling and brittle crushing/fracture of cell walls) and/or a combination of them, depending on the overall stress state. Current mechanism-based yield criteria usually consist of two or more failure envelopes with each representing a particular failure mechanism while the transition from one mechanism to another is generally ignored. For example, Gibson et al. (1989) derived a plastic yield surface for rigid foams, based on a plastic hinge analysis

$$\frac{\sigma_{vm}}{\sigma_{ys}} = \pm\gamma\left(\frac{\rho^*}{\rho_s}\right)^{3/2}\left\{1 - \left[\frac{3p}{\sigma_{ys}(\rho^*/\rho_s)}\right]^2\right\} \qquad (5a)$$

where p is the hydrostatic stress, σ_{vm} is the von Mises effective stress, and σ_{ys} is the yield strength of solid polymer. ρ^*/ρ_s is the foam relative density and γ is a material parameter to be determined from a uniaxial compression test. For PP foam (3.06 pcf), the material parameters calculated from simple compression results are: $\sigma_{ys} = 30$ MPa, $\rho^*/\rho_s = 0.05$, and $\gamma = 0.447$. In the $\sigma_{vm} - p$ space, Eq. 5(a) represents a fairly flat line as shown in Fig. 11(a). This curve must be truncated after some point when compressive stresses become dominant and the foam fails by elastic buckling. A theoretical buckling surface is also derived by Gibson et al. (1989) but without an analytical expression. Puso and Govindjee (1995) proposed following formula to fit the theoretical buckling surface by Gibson et al. (1989)

$$\sigma_{vm}^2 + \frac{1}{R^2}(p^2 - h^2) = 0 \qquad (5b)$$

where R and h can be determined from compression experiments.

Due to volumetric compressibility, the yield surface of crushable foams incorporates first and second stress invariants. In this study, the yield locus is defined by a single ellipse spanned on the plane of effective stress σ_{vm} and hydrostatic pressure p

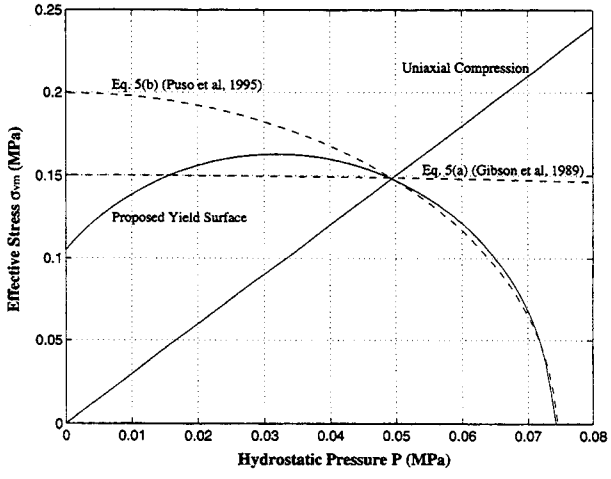

Fig. 11(a) Comparison between single-surface and multi-surface yield criteria

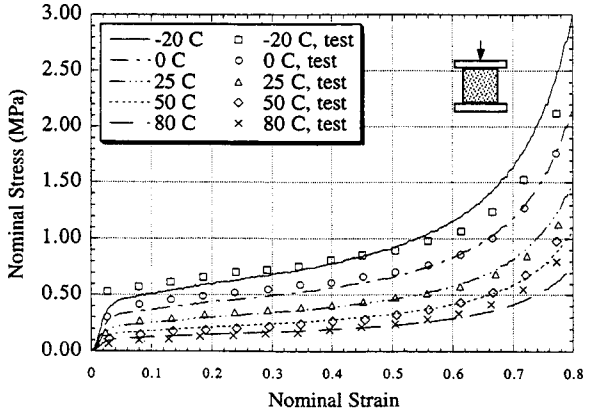

Fig. 10 Model predictions versus test results for PP Foam (3.06 pcf) at various temperatures

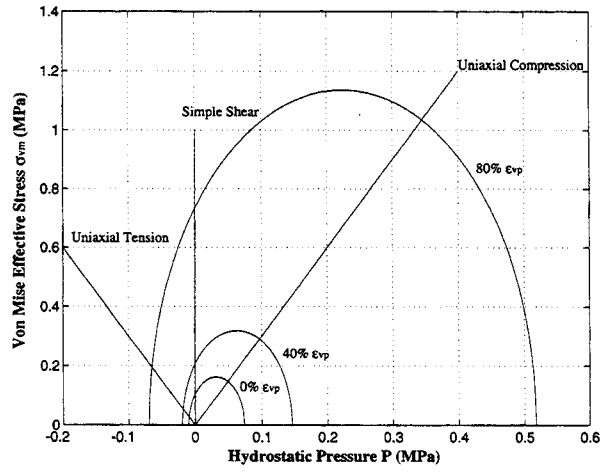

Fig. 11(b) Evolution of yield ellipse with increasing plastic volumetric strain

$$\frac{[p - x_0(\epsilon_{vp})]^2}{a(\epsilon_{vp})} + \frac{\sigma_{vm}^2}{b(\epsilon_{vp})} \leq 1 \tag{6}$$

where $x_0(\epsilon_{vp})$, $a(\epsilon_{vp})$, and $b(\epsilon_{vp})$ are three material parameters that define the center and the lengths of the major and minor axes of the yield ellipse. The yield ellipse is extendible in the hydrostatic pressure and effective stress space as a foam specimen densifies under loading, and can be uniquely defined by three types of tests: (1) uniaxial compression, (2) hydrostatic compression, and (3) simple shear. The initial yielding ellipse of PP foam (3.06 pcf, 5 percent relative density) is plotted in Fig. 11(*a*) along with the yield surface proposed by Gibson et al. (1989) and the buckling surface by Puso and Govindjee (1995). The buckling cap parameters calculated for the PP foam (3.06 pcf) from hydrostatic compression and uniaxial compression testing results are: $R = 0.364$ and $h = 0.074$ MPa. It can be seen from Fig. 11(*a*) that the phenomenological, single-surface yield criterion Eq. (6) agrees reasonable well with the multi-surface criteria defined by Eqs. (5*a*) and (5*b*). Within the low pressure range, only Eq. (5*a*) should be used for comparison since plastic yielding is presumably the dominant failure mechanism. The relatively large descrepancy in this range may come from the complex, irregular microstructure of this particular foam (ref. Fig. 1(*a*)). Since only three data points are available in the present study, at which the proposed model (6) are exact, it is hard to judge the accuracy of either model. Nevertheless, for compression-dominant impact problems, the proposed model appears to work well as can be seen from the structural simulation result later in this paper. Also, the single-surface criterion possesses no corner point and offers simplicity for numerical implementation. However, it can not be applied to orthotropic foams. Mechanism-based, orthotropic yield functions are included in Puso and Govindjee (1995) and Gibson et al. (1989). The evolution of the yield surface of the PP foam (3.06 pcf) with increasing plastic volumetric strain is depicted in Fig. 11(*b*).

3.3 Flow Rule. Low-density foam materials usually exhibit negligible lateral bulging after yielding during an uniaxial compression test. This indicates that foam materials, unlike metals, possess both volumetric plastic flow and shear flow. In the present study, the flow rule is defined by a non-associative flow potential in terms of hydrostatic and deviatoric effective stresses

$$g(\hat{\sigma}, \hat{q}) = \sqrt{\alpha p^2 + \sigma_{vm}^2} \tag{7}$$

where α is a material parameter that controls plastic volumetric flow. $\hat{q}$ is a general internal state variable, which is defined as the plastic volumetric strain in this case. The plastic strain rate tensor obeys the consistency condition

$$\hat{\dot{\epsilon}}_p = \dot{\lambda} \frac{\partial g(\hat{\sigma}, \hat{q})}{\partial \hat{\sigma}} \tag{8}$$

where $\dot{\lambda}$ is the consistency parameter. The plasticity theory requires the stress state be either inside or on the yield surface and $\dot{\lambda}$ can grow only when the stress state is on the yield surface. This allows us to solve $\dot{\lambda}$ by invoking the consistency condition Eq. (8) and the yield criterion Eq. (6).

For uniaxial compression in z-direction, the plastic Poisson's ratio ν_p is defined as

$$\dot{\epsilon}_{xxp} = \dot{\epsilon}_{yyp} = -\nu_p \dot{\epsilon}_{zzp} \tag{9}$$

and the plastic volumetric strain rate is written as

$$\dot{\epsilon}_{vp} = (1 - 2\nu_p)\dot{\epsilon}_{zzp} \tag{10}$$

Substituting Eq. (7) into Eq. (8), we have

$$\hat{\dot{\epsilon}}_p = \dot{\lambda} \frac{1}{2g} \left[2\sigma_{vm} \frac{\partial \sigma_{vm}}{\partial \hat{\sigma}} + 2\alpha p \frac{\partial p}{\partial \hat{\sigma}} \right] \tag{11}$$

This can be rewritten as

$$\hat{\dot{\epsilon}}_p = \dot{\lambda} \frac{3}{2g} \left[\hat{\mathbf{s}} - \frac{2\alpha}{9} p \hat{\mathbf{I}} \right] \tag{12}$$

For the uniaxial deformation case, the longitudinal and volumetric plastic strains are found by decomposition of Eq. (12)

$$\dot{\epsilon}_{zzp} = \dot{\lambda} \frac{3}{2g} \left(s_{zz} - \frac{2\alpha}{9} p \right) \tag{13}$$

$$\dot{\epsilon}_{vp} = -\dot{\lambda} \frac{\alpha p}{g} \tag{14}$$

The value of the longitudinal deviator s_{zz} is $-2p$. Substituting Eqs. (13) and (14) into Eq. (10), we have

$$\alpha = \frac{9(1 - 2\nu_p)}{2(1 + \nu_p)} \tag{15}$$

If $\alpha = \frac{9}{2}$, there will be no lateral plastic deformation during a uniaxial compression. To be physically admissible, the values of hydrostatic pressure multiplier should be limited within the range of $0 \leq \alpha \leq \frac{9}{2}$. The upper limit corresponds to zero Poisson's ratio. The lower limit corresponds to incompressible plasticity. For crushable foams with zero plastic Poisson's ratio, the flow potential can be written as (Bilkhu et al., 1993)

$$g = \sqrt{\tfrac{9}{2} p^2 + \sigma_{vm}^2} \tag{16}$$

3.4 Volumetric Hardening and Strain Rate Dependence. The volumetric hardening properties $x_0(\epsilon_{vp})$, $a(\epsilon_{vp})$, and $b(\epsilon_{vp})$ are defined by tabular stress-strain curve functions in terms of plastic volumetric strain based on experimental results.

Strain-rate effect is resulted from the gas flow and viscoplasticity of the cell wall properties (Gibson and Ashby, 1988). A phenomenological model with combined strain-rate hardening and temperature softening effects is given by Eq. (1). At room temperature, it can be generalized as

$$\dot{\bar{\epsilon}}_p = D\left(\frac{f}{f_0}\right)^{1/n}, \quad n = a + b\bar{\epsilon}_p \tag{17}$$

where f and f_0 are the effective yield stresses under an arbitrary and a reference quasi-static strain rate, respectively, and $\dot{\bar{\epsilon}}_p$ is the effective plastic strain rate defined as $\dot{\bar{\epsilon}}_p = \sqrt{\frac{2}{3}\dot{\epsilon}_{ij}^p \dot{\epsilon}_{ij}^p}$. For example, the calculated material parameters for the PP foam (3.06 pcf) are: $D = 0.768$, $a = 0.041$, and $b = 0.003$.

4 Numerical Implementation and Simulation

The above constitutive model was implemented into the finite element program LS-DYNA3D (Hallquist, 1994) as a user defined material subroutine. In this section, the numerical implementation procedures and applications of the current model will be presented.

4.1 Numerical Implementation. For transient analysis of large deformation impact problems, extreme small time steps need to be used. The stresses in each element are updated based on the constitutive law defined in last section at each time integration step.

First, the decomposed elastic trial stresses are calculated as

$$\hat{\mathbf{s}}_{n+1}^{trial} = \hat{\mathbf{s}}_n + 2G\hat{\dot{\epsilon}}_{d,n+(1/2)}\Delta t \tag{18}$$

$$p_{n+1}^{trial} = p_n - K\dot{\epsilon}_{v,n+(1/2)}\Delta t \tag{19}$$

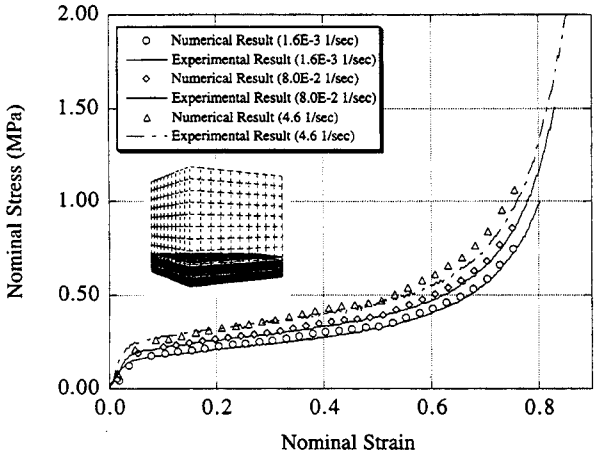

Fig. 12 Comparison between numerical and experimental results of polypropylene foam (3.06 pcf) under uniaxial compression

The trial elastic stresses and strains keep increasing until initial yielding happens. By using the one-step Euler backward return mapping algorithm (Hughes, 1983), the plastic consistency parameters are calculated. After each time step, the new yield surface is updated according to the plastic volumetric strain. Due to the adoption of the non-associative flow law, the return mapping path is not radial. The one-step Euler backward return mapping is of first order accuracy. For infinitesimal strain increment, the numerical error can be very small (Schreyer et al., 1979; Ortiz and Simo, 1986). The allowable post-yielding elastoplastic stresses are determined by

$$\hat{\sigma}_{n+1} = \hat{\sigma}^{trial}_{n+1} - 2G\hat{\epsilon}_{dp,n+(1/2)}\Delta t + K\dot{\epsilon}_{vp,n+(1/2)}\Delta t\hat{\mathbf{I}} \quad (20)$$

By splitting Eq. (20) into deviatoric and volumetric components, it becomes

$$\hat{\mathbf{s}}_{n+1} = \left(1 - 2G\dot{\lambda}\frac{3}{2g}\Delta t\right)\hat{\mathbf{s}}^{trial}_{n+1} = q\hat{\mathbf{s}}^{trial}_{n+1} \quad (21)$$

$$p_{n+1} = \left(1 - K\dot{\lambda}\frac{\alpha}{g}\Delta t\right)p^{trial}_{n+1} = \left(1 - 2G\dot{\lambda}\frac{3}{2g}\Delta t\frac{K\alpha}{3G}\right)p^{trial}_{n+1} \quad (22)$$

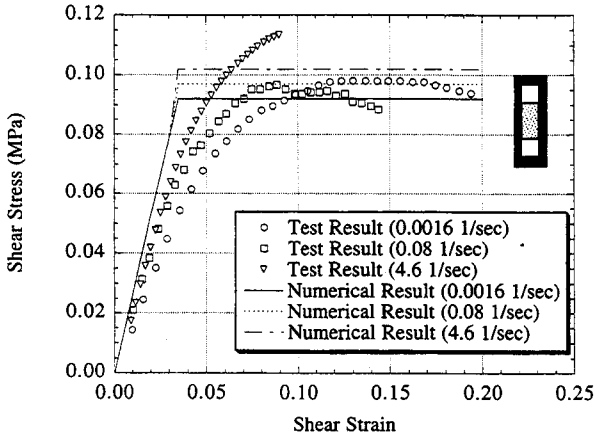

Fig. 13 Comparison between numerical and experimental results of polystyrene foam (1.0 pcf) under simple shear

where q is the stress correcting factor for deviatoric stress. These equations represent a stress projection from the elastic trial stress back onto the yield surface. The only unknown is the plastic flow multiplier $\dot{\lambda}$.

The plastic flow multiplier can be calculated by invoking the consistency condition and the yield criterion. For a crushable foam with zero Poisson's ratio, the stress correcting factors for the pressure and deviator are identical when $\alpha = \frac{9}{2}$ since

$$\alpha = \frac{3G}{K} = \frac{9(1-2\nu)}{2(1+\nu)} \quad (23)$$

By inserting Eqs. (21) and (22) into the yield criterion Eq. (6), we obtain a quadratic equation in terms of plastic stress correcting factor q

$$c_1q^2 + c_2q + c_3 = 0 \quad (24)$$

where

$$c_1 = \frac{\sigma^{trial^2}_{vm}}{b} + \frac{p^{trial^2}}{a} \quad (25)$$

$$c_2 = -\frac{2x_0p^{trial}}{a} \quad (26)$$

$$c_3 = \frac{x_0^2}{a} - 1 \quad (27)$$

Consequently, there are two real roots

$$q_{1,2} = \frac{-c_2 \pm \sqrt{c_2^2 - 4c_1c_3}}{2c_1} \quad (28)$$

The stress correcting factor should be the positive root.

In a general case when the material Poisson's ratio is not zero, the Euler backward return mapping algorithm can be rewritten as

$$\hat{s}_{n+1} = (1-w)\hat{s}^{trial}_{n+1} \quad (29)$$

$$p_{n+1} = \left(1 - w\frac{K\alpha}{3G}\right)p^{trial}_{n+1} \quad (30)$$

From Eqs. (29), (30), and (6), two roots $w_{1,2}$ for the resulted quadratic equation can be obtained. The introduction of nonassociative flow law may cause the non-uniqueness of solution. Since the return path is no longer radial, the return path may not intersect with the yield ellipse. Therefore, a non-associative flow law does not guarantee a physically admissible solution.

4.2 Numerical Simulation. The constitutive equations derived were implemented into LS-DYNA3D (Hallquist, 1994) via a user defined material subroutine. Numerical simulations are conducted to validate the constitutive model under different loading conditions. The material parameters are calibrated from experimental results discussed in the previous sections. The initial yield locus at zero plastic strain can be obtained from: (1) uniaxial compressive strength σ_0, (2) hydrostatic compressive

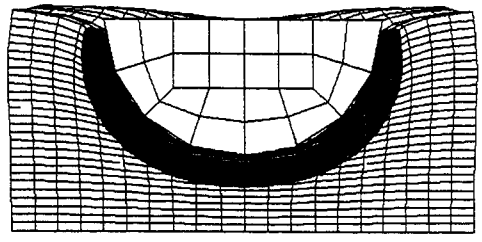

Fig. 14 Deformed mesh of PP foam (3.06 pcf) in the indentation test (at 4.5 m/s)

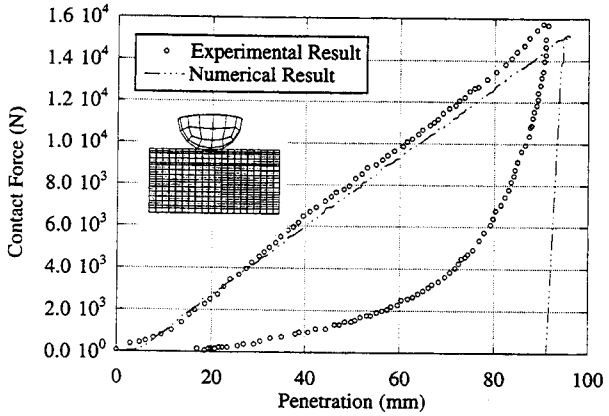

Fig. 15 Contact force-deflection responses: experiment versus simulation

strength p_{c0}, and (3) simple shear strength τ_0. For the PP foam (3.06 pcf), these parameters are: $\sigma_0 = 0.15$ MPa, $p_{c0} = 0.074$ MPa, and $\tau_0 = 0.058$ MPa. The hardening behavior is defined by three tabular functions $x_0(\epsilon_{vp})$, $a(\epsilon_{vp})$, and $b(\epsilon_{vp})$. The strain rate dependence is defined by Eq. (17).

Numerical simulations were performed to simulate homogeneous deformation modes and compared with experimental results. Figure 12 shows the comparison between simulated and measured stress-strain responses of the PP foam (3.06 pcf) under uniaxial compression at three different rates. A deformed configuration without lateral expansion is also shown in the insert of Fig. 12. Figure 13 shows both simulation and test results for the PS foam (1.0 pcf) subjected to simple shear. The after yielding behavior is perfect plastic because there is no volumetric strain hardening during the deformation.

For a more complicated loading case, the result from a high speed indentation test is used as a comparison with simulation result. During the test, a rigid hemisphere (ϕ127 mm, 22.2 kgm) is dropped onto a foam block (203 × 203 × 101 mm^3) with an initial speed of 4.5 m/s (10 mph). Figure 14 shows the deformed configuration of the PP foam block (3.06 pcf) during the impact. Contact forces versus deflection curves are plotted in Fig. 15. Good agreement between the experimental result and the simulation result is found for the loading stage. Since the current model assumes elastic unloading, large discrepancy is shown for the unloading stage. Further research is needed to model the unloading behavior of the foam materials accurately.

5 Concluding Remarks

(1) Polymeric foams investigated in this study are sensitive to strain rate and temperature. Their strain hardening, strain rate hardening and temperature dependent constitutive behaviors have been quantified by experiments.

(2) A phenomenological constitutive equation represents the strain-rate and temperature dependence of polypropylene foam (3.06 pcf) quite well.

(3) A hydrodynamic elastoplastic constitutive model that features a single-surface yield criterion, a nonassociated plastic flow law and a power-type strain-rate dependence showed reasonably good predictive capability for the responses of rigid polymeric foams under simple and complex loading conditions (e.g., Figs. 12 to 15).

(4) The tensile failure of polymeric foams has not been adequately treated by the current model although it is less relevant for targeted applications in compression dominant crash impacts. Also, the unloading behaviors of the polymeric foams have not been accurately modeled. Further refinements are therefore needed to improve the model.

Acknowledgments

This research has been supported by a grant from American Automobile Manufacturers Association (AAMA). However, the analysis and conclusions contained in this paper are solely those of the authors and have not been reviewed or approved by AAMA. Special thanks to Livermore Software Technology Corporation for the use of LS-DYNA3D software in numerical investigations presented in this study. We are also grateful to two anonymous reviewers for their valuable comments and suggestions.

References

Barbat, S. D., and Prasad, P., 1995, "Finite Element Modeling of Structural Foam and Head Impact Interaction with Vehicle Upper Interior," SAE paper 950885, pp. 173–184.

Bilkhu, S. S., Founnas, M., and Nusholtz, G. S., 1993, "Material Modeling of Structure Foams in Finite Element Analysis Using Compressive Uniaxial and Triaxial Data," SAE Technical Paper Series 930434, International Congress and Exposition, Detroit, MI.

Chang, F. S., Hallquist J. O., Lu, D. X., Shahidi, B. K., Kudelko, C. M and Tekelly, J. P., 1994, "Finite Element Analysis of Low-Density High-hysteresis Foam Materials and the Application in the Automotive Industry," SAE paper 940908, pp. 71–78.

Gibson, L. J., and Ashby, M. F., 1988, *Cellular Solids-Structural and Properties*, Pergamon Press, New York.

Gibson, L. J., Zhang, J., Shercliff, T. L., Gibson, L. J., and Ashby, M. F., 1989, "Failure Surface for Cellular Materials under Multiaxial Loads-I. Modeling," *International Journal of Mechanical Science*, Vol. 31, No. 9, pp. 635–663.

Hallquist, J. O., 1994, *LS-DYNA3D Theoretical Manual*, LSTC Report 1018.

Hughes, J. R., 1983, "Numerical Implementation of Constitutive Models: Rate-Independent Deviatoric Plasticity," Workshop on the Theoretical Foundation for Large-Scale Computations of Nonlinear Material Behavior, Northwestern University, Evanston, IL, Oct.

Krieg, R. D., 1972, "A Simple Constitutive Description for Soils and Crushable Foam," SCDR-72-0883, Sandia National Laboratories, Albuquerque, NM.

Nagy, A., Ko, W. L., and Lindholm, U. S., 1964, "Mechanical Behavior of Foamed Materials under Dynamic Compression," *Journals of Cellular Plastics*, Vol. 10, pp. 127–134.

Neilsen, M. K., Krieg, R. D., and Schreyer, H. L., 1995, "A Constitutive Theory for Rigid Polyurethane Foam," *Polymer Engineering and Science*, Vol. 35, pp. 387–394.

Ortiz, M., and Simo, J. C., 1986, "An Analysis of a New Class of Integration Algorithms for Elastoplastic Constitutive Relations," *International Journal for Numerical Methods in Engineering*, Vol. 23, pp. 353–366.

Patel, M. R. and Finnie, I., 1969, The Deformation and Fracture of Rigid Cellular Plastics under Multiaxial Stress, Lawrence Livermore National Laboratories, Albuquerque, NM, SAND86-2927.

Puso, M. A. and Govindjee, 1995, "A Phenomenological Constitutive Model for Polymeric Foam," *Mechanics of Plastics and Plastic Composites*, MD-Vol. 68/AMD-Vol. 215, ASME, pp. 159–176.

Ramon, O., Mirahi, S., and Miltz, J., 1990, "Mechanical Properties and Behavior of Open Cell Foams Used as Cushioning Materials," *Polymer Engineering and Science*, Vol. 30, pp. 197–201.

Rush, K. C., 1969, "Load-Compression Behavior of Flexible Foams," *Journal of Applied Polymer Science*, Vol. 13, pp. 2297–2311.

Shaw, M. C. and Sata, T., 1966, "The Plastic Behavior of Cellular Materials," *International Journal of Mechanical Science*, Vol. 8, pp. 469.

Schofield, A. and Worth, C. P., 1968, *Critical State Soil Mechanics*, McGraw-Hill, New York.

Schreyer, H. L., Kulak, R. F., and Kramer, J. M., 1979 "Accurate Numerical Solutions for Elastic-Plastic Models," ASME *Journal of Pressure Vessel Technology*, Vol. 101.

Sherwood J. A., and Frost, C. C., 1992, "Constitutive Modeling and Simulation of Energy Absorbing Polyurethane Foam under Impact Loading," *Polymer Engineering and Science*, pp. 1138–1146, Vol. 32, No. 16.

Triantafillou, T. C., Zhang, J., Shercliff, T. L., Gibson, L. J., and Ashby, M. F., 1989, "Failure Surfaces for Cellular Materials under Multiaxial Loads-II. Comparisons of Models with Experiment," *International Journal of Mechanical Science*, Vol. 31, No. 9, pp. 665–678.

Triantafillou, T. C., and Gibson, L. J., 1990, "Multiaxial Failure Criteria for Brittle Foams," *International Journal of Mechanical Science*, Vol. 32, No. 6, pp. 479–496.